Galectin-3 Deficiency Accelerates High-Fat Diet–Induced Obesity and Amplifies Inflammation in Adipose Tissue and Pancreatic Islets

Nada N. Pejnovic,[1,2] Jelena M. Pantic,[1] Ivan P. Jovanovic,[1] Gordana D. Radosavljevic,[1] Marija Z. Milovanovic,[1] Ivana G. Nikolic,[4] Nemanja S. Zdravkovic,[1] Aleksandar L. Djukic,[2,3] Nebojsa N. Arsenijevic,[1] and Miodrag L. Lukic[1]

Obesity-induced diabetes is associated with low-grade inflammation in adipose tissue and macrophage infiltration of islets. We show that ablation of galectin-3 (Gal-3), a galactoside-binding lectin, accelerates high-fat diet–induced obesity and diabetes. Obese *LGALS3*$^{-/-}$ mice have increased body weight, amount of total visceral adipose tissue (VAT), fasting blood glucose and insulin levels, homeostasis model assessment of insulin resistance, and markers of systemic inflammation compared with diet-matched wild-type (WT) animals. VAT of obese *LGALS3*$^{-/-}$ mice exhibited increased incidence of type 1 T and NKT lymphocytes and proinflammatory CD11c^{+}CD11b^{+} macrophages and decreased CD4^{+}CD25^{+}FoxP3^{+} regulatory T cells and M2 macrophages. Pronounced mononuclear cell infiltrate, increased expression of NLRP3 inflammasome and interleukin-1β (IL-1β) in macrophages, and increased accumulation of advanced glycation end products (AGEs) and receptor for AGE (RAGE) expression were present in pancreatic islets of obese *LGALS3*$^{-/-}$ animals accompanied with elevated phosphorylated nuclear factor-κB (NF-κB) p65 and mature caspase-1 protein expression in pancreatic tissue and VAT. In vitro stimulation of *LGALS3*$^{-/-}$ peritoneal macrophages with lipopolysaccharide (LPS) and saturated fatty acid palmitate caused increased caspase-1–dependent IL-1β production and increased phosphorylation of NF-κB p65 compared with WT cells. Transfection of *LGALS3*$^{-/-}$ macrophages with NLRP3 small interfering RNA attenuated IL-1β production in response to palmitate and LPS plus palmitate. Obtained results suggest important protective roles for Gal-3 in obesity-induced inflammation and diabetes. ***Diabetes*** **62:1932–1944, 2013**

Metabolic inflammation, "metaflammation," is a chronic, low-grade adipose tissue inflammation triggered by various metabolic "danger" signals during obesity that precedes the development of insulin resistance and type 2 diabetes (1). Adipose tissue–associated regulatory T cells (Tregs), type 2 T helper cells, and alternatively activated M2 macrophages protect from the instigation of nutrient excess–induced inflammation (2), whereas the recruitment of type 1 T helper lymphocytes and M1 macrophages and decreased Tregs in adipose tissue precede metabolic disorders (3,4). Proinflammatory interleukin-1β (IL-1β) and tumor necrosis factor-α impair insulin sensitivity, but molecular pathways that associate inflammation, diet, and type 2 diabetes are not fully understood (5). It has been postulated that the activation of nuclear factor-κB (NF-κB), a family of transcription factors that regulate the expression of proinflammatory genes upon cell stimulation with various factors including hyperglycemia and free fatty acids, is a molecular mechanism involved in insulin resistance (6). Most recently, the crucial role for the NLRP3 inflammasome, which consists of NLRP3 molecules, adaptor protein ASC, and procaspase-1 that catalytically activates caspase-1, causing the release of IL-1β and IL-18, was demonstrated in studies in which the ablation of the NLRP3 inflammasome prevented obesity-induced inflammation and insulin resistance (7–9).

Galectin-3 (Gal-3; also known as Mac-2), a 30-kDa β-galactoside–binding lectin, mainly located in the cytoplasm, but also in the nucleus, is expressed by a variety of cell types and regulates various T-cell functions and innate immune responses (10). Gal-3 plays an important disease-exacerbating role in autoimmune/inflammatory and malignant diseases (11–14). Gal-3 is also one of the pattern recognition receptors that bind and mediate the degradation of modified lipoproteins and advanced glycation end products (AGEs) (15). In contrast to other receptors for AGE (RAGEs), Gal-3 acts to protect from AGE-induced tissue injury. Therefore, Gal-3 ablation accelerates AGE-induced kidney injury in diabetes (16) and enhances atherogenesis (17). Gal-3 protects β-cells from the cytotoxic effect of IL-1β in rats (18) and its increased expression was demonstrated in islet endothelial cells in obesity-induced diabetes in mice (19).

The aim of this study was to investigate the role of Gal-3 in high-fat diet (HFD)–induced obesity and associated metabolic abnormalities by using mice lacking Gal-3 on a C57BL/6 background. We report here that Gal-3 ablation accelerated HFD-induced obesity and amplified inflammation in adipose tissue and pancreatic islets.

RESEARCH DESIGN AND METHODS

Experimental mice. Male Gal-3–deficient (*LGALS3*$^{-/-}$) mice on the C57BL/6 background and their littermate controls, wild-type (WT) C57BL/6 mice (6 weeks of age), obtained from the University of California Davis (Davis, CA; by courtesy of D.K. Hsu and F.T. Liu) were fed either a low-fat diet (LFD; 3% fat) or HFD (60% fat) obtained from Mucedola (Milano, Italy) for 11 or 18 weeks. All animal procedures were approved by the ethical committee (04/11) of the Faculty of Medical Sciences, University of Kragujevac.

Metabolic parameters. Body weights and fasting blood glucose levels were measured once every 2 weeks. Mice were fasted for 4 h, and glucose levels (mmol/L) were determined using the Accu-Chek Performa glucometer (Roche

From the [1]Center for Molecular Medicine and Stem Cell Research, Kragujevac, Serbia; the [2]Institute of Pathophysiology, Faculty of Medical Sciences, University of Kragujevac, Kragujevac, Serbia; the [3]Center for Endocrinology, Diabetes, and Metabolic Diseases, Clinical Center Kragujevac, Kragujevac, Serbia; and the [4]Department of Immunology, Institute for Biological Research "Sinisa Stankovic," University of Belgrade, Belgrade, Serbia.
Corresponding author: Miodrag L. Lukic, miodrag.lukic@medf.kg.ac.rs.
Received 22 February 2012 and accepted 3 January 2013.
DOI: 10.2337/db12-0222
N.N.P. and J.M.P. contributed equally to this study.

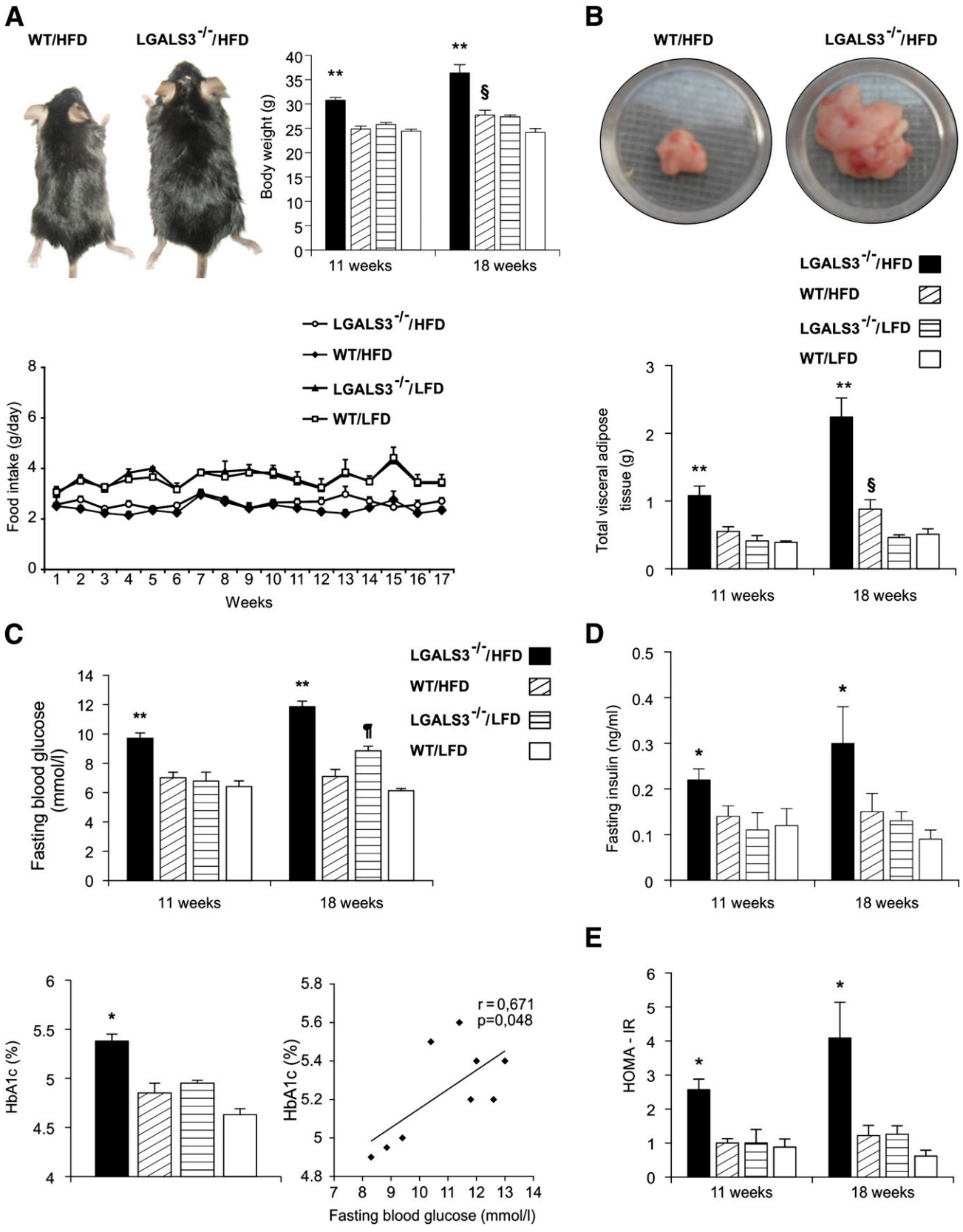

FIG. 1. ***LGALS3*$^{-/-}$ mice fed HFD have increased body weight, enhanced visceral adiposity, hyperglycemia, hyperinsulinemia, and increased HOMA-IR.** ***A*: An image of the larger body size of *LGALS3*$^{-/-}$ vs. WT mice fed HFD. A significant increase in body weights of HFD-fed *LGALS3*$^{-/-}$ mice compared with other experimental groups after 11 or 18 weeks, and WT mice fed HFD vs. WT mice fed LFD after 18 weeks. Food intake in *LGALS3*$^{-/-}$ and WT mice. *B*: Significantly increased amount of VAT in HFD-fed *LGALS3*$^{-/-}$ mice vs. other experimental groups after 11 or 18 weeks and WT mice on different diets after 18 weeks. *C*: Significant hyperglycemia of *LGALS3*$^{-/-}$ mice on HFD compared with other experimental groups after 11 or 18 weeks and LFD-fed *LGALS3*$^{-/-}$ vs. WT mice after 18 weeks. Increased HbA_{1c} (%) of *LGALS3*$^{-/-}$ mice on HFD vs. other experimental groups, which significantly correlates with fasting blood glucose levels in *LGALS3*$^{-/-}$ mice ($r = 0.671$, $P = 0.048$). *D*: Significant increase of fasting**

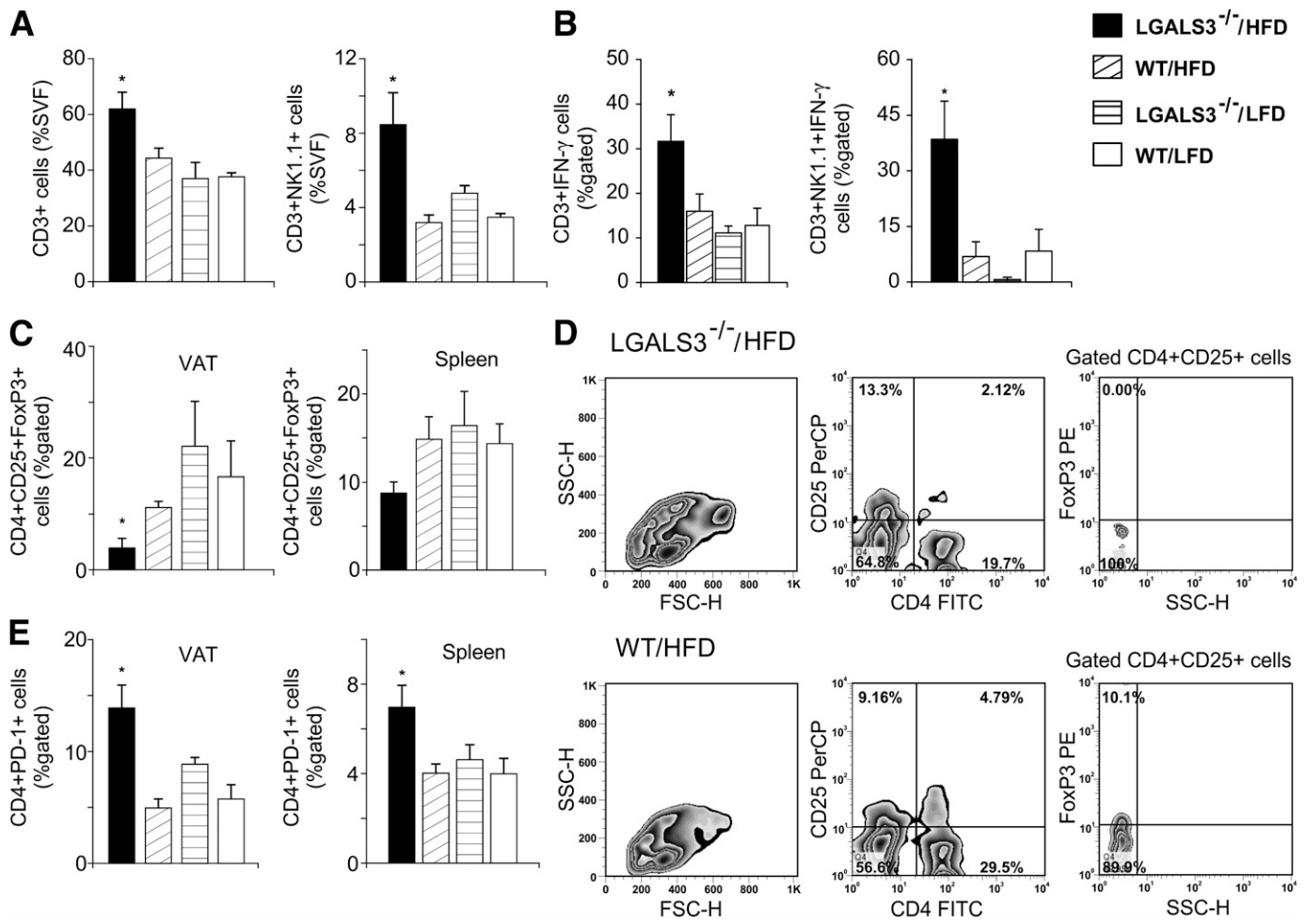

FIG. 2. Increased type 1 T and NKT cells and reduced Tregs in VAT of HFD-fed *LGALS3*$^{-/-}$ mice. *A*: Increased percentages of CD3$^+$ T cells and in VAT of *LGALS3*$^{-/-}$ mice fed HFD compared with other groups after 11 weeks. CD3$^+$NK1.1$^+$ NKT cells in VAT of *LGALS3*$^{-/-}$ mice fed HFD were significantly increased compared with WT mice on both diet conditions. *B*: *LGALS3*$^{-/-}$ mice fed HFD have significantly increased frequencies of CD3$^+$IFN-γ$^+$ in VAT compared with LFD-fed mice of both genotypes, whereas CD3$^+$NK1.1$^+$ NKT cells that express IFN-γ were significantly higher compared with other experimental groups. *C*: Adipose tissue regulatory CD4$^+$CD25$^+$FoxP3$^+$ T cells are reduced, and the trend toward decreased Tregs is observed in spleens ($P = 0.071$) of *LGALS3*$^{-/-}$ vs. WT mice fed HFD. *D*: Representative fluorescence-activated cell sorter plot of CD4$^+$CD25$^+$FoxP3$^+$ T cells in VAT from HFD-fed *LGALS3*$^{-/-}$ and WT mice. *E*: Significantly increased percentages of CD4$^+$PD-1$^+$ cells in VAT and spleen from HFD-fed *LGALS3*$^{-/-}$ mice vs. WT mice on both diet conditions. The results are shown as the means ± SEM for four to six animals per group. FSC-H, forward-scattered light; FITC, fluorescein isothiocyanate; SSC-H, side-scattered light in flow cytometry; SVF, stromal vascular fraction. *$P < 0.05$.

Diagnostics, Mannheim, Germany). Serum concentrations of lipids and HbA_{1c} were measured using the Olympus AU600 Chemistry Immuno Analyzer (Olympus, Tokyo, Japan) and fasting insulin in sera using the Rat/Mouse Insulin ELISA Kit (Millipore Corporation, Billerica, MA). Homeostasis model assessment of insulin resistance (HOMA-IR) was calculated as previously described (20).

Isolation of visceral adipose tissue stromal vascular fraction cells. Total visceral adipose tissue (VAT) was minced, placed in PBS containing 1 mg/mL collagenase type II and 2% BSA (Sigma-Aldrich, St. Louis, MO), incubated for 1 h in a water bath at 37°C, and passed through a 40-μm nylon cell strainer (BD Biosciences, San Jose, CA) to enrich stromal vascular fraction cells.

Isolation of pancreatic mononuclear cells. Dissected pancreata were pooled, minced, and digested using 2 mg/mL collagenase type V in Hanks' balanced salt solution (Sigma-Aldrich) with 10% FCS for 15 min in a water bath at 37°C (21), and digests were passed through a 40-μm cell strainer.

Isolation of splenocytes. Spleens were excised and single-cell suspensions were obtained by mechanical disruption and lysis of RBCs.

Flow cytometry. Cells were labeled with fluorochrome-conjugated monoclonal antibodies: anti-mouse CD3, CD4, CD8, CD44, CD62L, CD279 (PD-1), CD11b, interferon-γ (IFN-γ), IL-17 (BD Biosciences), NK1.1, F4/80, CD206, and CD11c antibodies (BioLegend, San Diego, CA). For intracellular staining, cells were activated with PMA/ionomycin and processed as previously described (22). Primary rabbit anti-mouse NLRP3, IL-1β, and NF-κB (phospho-S536) antibody (1 μg/mL; Abcam, Cambridge, U.K.) and secondary goat anti-rabbit antibody labeled with PE-Cy5.5 (1/400; Invitrogen, Carlsbad, CA) were used. Cells were analyzed with the FACSCalibur Flow Cytometer (BD Biosciences), and analysis was conducted with FlowJo (Tree Star).

Pancreatic histology and insulitis scoring. Pancreatic tissue cryostat sections were stained with hematoxylin-eosin. Histological analysis of the distribution of inflammatory cell infiltrate in pancreatic islets was performed in blinded fashion by two independent observers. The images were captured with a light microscope (BX51; Olympus) equipped with a digital camera. Insulitis was graded and a mean insulitis score was calculated (23).

Immunofluorescent staining. Immunofluorescent staining of pancreatic tissue cryosections (5 μm) was performed using rabbit anti-mouse NLRP3 (1:200), IL-1β (1:200), IL-18 (1:200), RAGE (1:400), and AGE (1:200) antibodies (Abcam), followed by incubation with goat anti-rabbit IgG antibody PE-Cy 5.5, followed by FITC-conjugated anti-mouse insulin antibody (1:400; Abcam). The

insulin levels in sera of *LGALS3*$^{-/-}$ fed HFD vs. other experimental groups after 11 or 18 weeks. *E*: Significant increase of HOMA-IR in HFD-fed *LGALS3*$^{-/-}$ mice compared with other experimental groups after 11 or 18 weeks. The results are shown as the means ± SEM for 8–12 animals (11 weeks) or four to seven mice (18 weeks) per group. *r*, Pearson correlation coefficient. *$P < 0.05$; **$P < 0.001$; ¶$P < 0.05$; §$P < 0.05$. (A high-quality color representation of this figure is available in the online issue.)

sections were mounted with ProLong Gold antifade reagent with DAPI (Invitrogen) and analyzed at ×40 magnification using the Nikon Eclipse Ti-E inverted research microscope equipped with NIS-Elements Imaging software (Nikon Instruments Inc., Melville, NY). Only brightness and contrast were adjusted.

Immunohistochemistry. Pancreatic tissue cryosections were incubated with biotinylated F4/80 antibody (Invitrogen) followed by visualization using the Mouse-Specific HRP/DAB Detection IHC Kit (Abcam). Next, they were incubated with rabbit anti-mouse NLRP3, IL-1β, AGE, RAGE, and Gal-3, visualized by rabbit-specific conjugate (Expose Rb-Specific HRP/AEC Detection IHC Kit; Abcam), photomicrographed with a digital camera mounted on light microscope (Olympus BX51), digitized, and analyzed (24). Results are expressed as percent positive staining in the specified region.

Cell culture. Macrophages were collected from the peritoneal cavity of mice under sterile conditions and cultured in complete Dulbecco's modified Eagle's medium supplemented with 10% FCS at 37°C in a 5% CO_2 incubator. After pretreatment with lipopolysaccharide (LPS) (100 ng/mL) for 4 h, cells were stimulated with BSA alone or palmitate-BSA (100 μmol/L), glucose (22 mmol/L), and H_2O_2 (10 μmol/L) (all from Sigma-Aldrich) for 24 h. Where indicated, cells were preincubated with the caspase-1 inhibitor Z-YVAD-FMK (10 μmol/L; Bachem AG, Bubendorf, Switzerland).

Caspase-1 activity assay. For the determination of caspase-1 activity, we used the Caspase-1 Colorimetric Kit (R&D Systems) according to the manufacturer's recommendations.

NLRP3 knockdown with small interfering RNA transfection. Peritoneal macrophages were seeded on six-well plates (1×10^6 cells/well), washed once with 2 mL small interfering RNA (siRNA) transfection medium, transfected with 60 pmol NLRP3 siRNA or 60 pmol negative control siRNA, and incubated for 7 h according to the manufacturer's instructions (Santa Cruz Biotechnology, Santa Cruz, CA).

Western blot. Pancreatic tissue lysates were prepared in a solution containing 62.5 mmol/L Tris-HCl, pH 6.8, 2% weight/volume (wt/vol) SDS, 10% glycerol, 50 mmol/L dithiothreitol, 0.01% wt/vol bromophenol blue, 1 mmol/L phenylmethylsulphonyl fluoride, 1 μg/mL aprotonin, and 2 mmol/L EDTA, and proteins from VAT were isolated with TRIzol reagent (Genosys, Woodlands, TX) and further processed (25). Rabbit polyclonal IgG antibodies to ASC (1:500), NLRP3 (1:500), IL-1β (1:2500), caspase-1 (1:500), NF-κB p65 (phospho-S536) (1:500), and NF-κB p65 (1:500) (all from Abcam) and mouse anti-mouse IgG1 β-actin antibody (1:500) (Sigma-Aldrich) as internal control were used, followed by donkey anti-rabbit horseradish peroxidase at 1:10,000 or sheep anti-mouse horseradish peroxidase (1:2,500) (GE Healthcare, Buckinghamshire, U.K.). Detection was performed by chemiluminescence (ECL; GE Healthcare), and photographs were made by X-ray films (Kodak). Scion Image Alpha 4.0.3.2 (Scion Corporation, Frederick, MD) was used to calculate protein expression.

Cytokine measurement. Cytokine levels were determined using mouse duo sets for IL-1β/IL-1F2, IL-6, IL-4, IL-13, IL-10, IFN-γ, IL-17, and CRP (R&D Systems, Minneapolis, MN, USA) according to the manufacturer's recommendations.

Statistical analyses. All data are presented as means ± SEM. Statistical significance was determined by ANOVA (one-way ANOVA and Bonferroni post hoc test), independent-sample Student t test, and, where appropriate, Kruskal-Wallis and Mann-Whitney U test. Relationships between variables were assessed using Pearson correlation. Statistical significance was assumed at $P < 0.05$. Statistical analyses were performed using SPSS 13.0.

RESULTS

Lack of Gal-3 accelerates HFD-induced obesity and obesity-related metabolic abnormalities. Body weight (Fig. 1*A*) and total VAT weight (Fig. 1*B*) were significantly higher in HFD-fed *LGALS3*$^{-/-}$ mice compared with other experimental groups at both 11 and 18 weeks, and significantly greater in WT mice on HFD versus LFD at 18 weeks

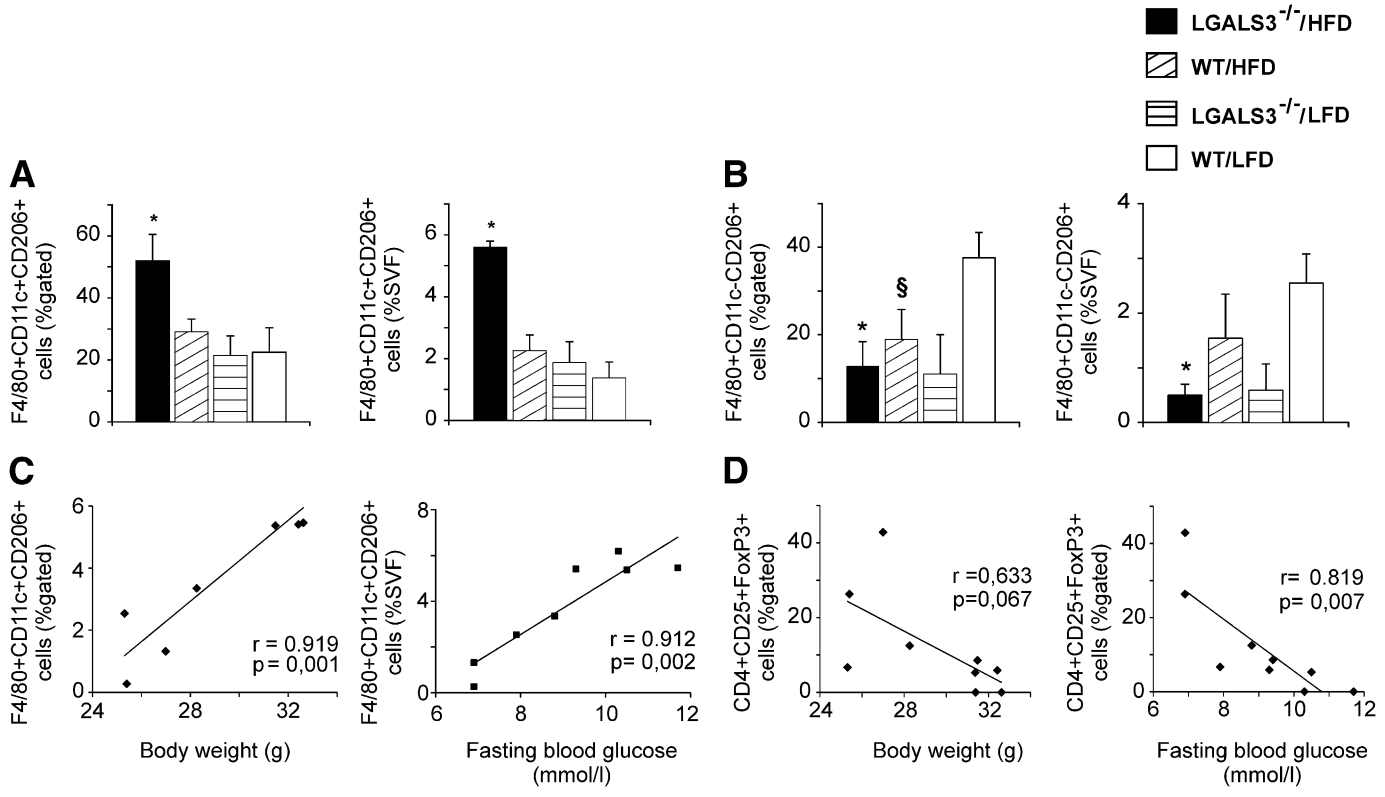

FIG. 3. Increased frequencies of adipose tissue F4/80$^+$CD11c$^+$CD206$^+$ macrophages in obese *LGALS3*$^{-/-}$ mice correlate with body weights and blood glucose levels in *LGALS3*$^{-/-}$ mice. *A*: *LGALS3*$^{-/-}$ mice fed HFD for 11 weeks have significantly increased percentages of F4/80$^+$CD11c$^+$CD206$^+$ macrophages in VAT compared with other experimental groups. *B*: *LGALS3*$^{-/-}$ fed HFD have significantly lower percentages of alternatively activated F4/80$^+$CD11c-CD206$^+$ M2 macrophages in VAT compared with WT mice fed LFD. *C*: Positive correlation between the frequencies of proinflammatory F4/80$^+$CD11c$^+$CD206$^+$ macrophages with body weights (r = 0.919, P = 0.001) and fasting blood glucose levels (r = 0.912, P = 0.002) in *LGALS3*$^{-/-}$ mice. *D*: Inverse correlation between the frequencies of Tregs with body weights (r = 0.633, P = 0.067) and blood glucose levels (r = 0.819, P = 0.007) in *LGALS3*$^{-/-}$ mice. r, Pearson correlation coefficient. The results are shown as the means ± SEM for four to six animals per group. SVF, stromal vascular fraction. *$P < 0.05$; §$P < 0.05$.

(Fig. 1*A* and *B*). There was no difference in food intake between *LGALS3*$^{-/-}$ and WT mice (Fig. 1*A*). Fasting blood glucose levels and insulinemia and HbA_{1c} were significantly increased in HFD-fed *LGALS3*$^{-/-}$ mice compared with other experimental groups at both 11 and 18 weeks, whereas in WT mice on HFD versus LFD at 18 weeks, the differences did not reach statistical significance (Fig. 1*C* and *D*). Hyperglycemia was noticed in *LGALS3*$^{-/-}$ mice fed LFD at 18 weeks (Fig. 1*C*). Of note, the significantly increased body weight (26.25 ± 0.66 vs. 22.19 ± 0.67 g, P = 0.010) and fasting glycemia (8.92 ± 0.47 vs. 6.82 ± 0.31 mmol/L, P = 0.004) were already noticed after 3 weeks of HFD in *LGALS3*$^{-/-}$ mice compared with diet-matched WT mice. HbA_{1c} (%) and fasting glycemia significantly correlated in *LGALS3*$^{-/-}$ mice at 18 weeks (Fig. 1*C*). HOMA-IR was significantly higher in HFD-fed *LGALS3*$^{-/-}$ mice compared with other experimental groups at 11 and 18 weeks (Fig. 1*E*). Total, HDL, and non-HDL cholesterol serum levels increased with HFD but were not significantly different between the genotypes, and serum levels of triglycerides were similar between experimental groups at 11 weeks (data not shown).

Type 1 T/NKT cells are increased in VAT in obese *LGALS3*$^{-/-}$ mice. Significantly increased $CD3^+$ T cells and $CD3^+NK1.1^+$ NKT cells were found in VAT in HFD-fed *LGALS3*$^{-/-}$ mice (Fig. 2*A*) with markedly increased $CD3^+NK1.1^+$ IFN-γ^+ type 1 NKT cells, and $CD3^+$IFN-γ^+ type 1 T cells were significantly higher compared with LFD-fed mice of both genotypes at 11 weeks (Fig. 2*B*). The incidence of $CD4^+$ or $CD8^+$ T-naïve, memory or effector populations and $CD3^+$IL-17$^+$ cells was not different between groups (data not shown). $CD4^+CD25^+FoxP3^+$ Tregs were significantly lower in the VAT and spleens (P = 0.071) of obese *LGALS3*$^{-/-}$ mice compared with other experimental groups (Fig. 2*C* and *D*). $CD4^+$PD-1$^+$ cells were significantly increased in the VAT and spleens with HFD in *LGALS3*$^{-/-}$ mice (Fig. 2*E*).

Increased proinflammatory and reduced alternatively activated M2 macrophages in VAT of obese *LGALS3*$^{-/-}$ mice. We next monitored the recruitment of macrophages into adipose tissue after 11 weeks on HFD to look for potential mechanisms of glucose metabolism abnormalities in obese *LGALS3*$^{-/-}$ mice. Proinflammatory F4/80$^+$CD11c$^+$CD206$^+$ macrophages significantly increased in adipose tissue of *LGALS3*$^{-/-}$ mice fed HFD compared with other experimental groups (Fig. 3*A*). HFD increased splenic F4/80$^+$CD11b$^+$CD11c$^+$ bone marrow–derived dendritic cells (BMDCs) in mice of both genotypes (data not shown). After 18 weeks on HFD, adipose tissue BMDCs were significantly higher in *LGALS3*$^{-/-}$ compared with WT mice (72.63 ± 3.91 vs. 38.04 ± 10.54, P = 0.006). Alternatively, activated F4/80$^+$CD11c$^-$CD206$^+$ M2 macrophages were markedly reduced in VAT from both *LGALS3*$^{-/-}$ and WT mice fed HFD compared with LFD-fed WT mice at 11 weeks (Fig. 2*B*), and further decreased in *LGALS3*$^{-/-}$ mice fed HFD for 18 weeks, significantly lower compared with diet-matched WT mice (0.93 ± 0.093 vs. 7.66 ± 2.99, P = 0.046).

Body weights and fasting glycemia correlate with adipose tissue proinflammatory macrophages and Tregs in *LGALS3*$^{-/-}$ mice. In *LGALS3*$^{-/-}$ mice, proinflammatory F4/80$^+$CD11c$^+$CD206$^+$ adipose tissue macrophages significantly correlated with body weight (r = 0.919, P = 0.001) and fasting blood glucose levels (r = 0.912, P = 0.002) (Fig. 3*C*), whereas Tregs inversely correlated with body weight (r = 0.633, P = 0.067) and fasting glycemia (r = 0.819, P = 0.007) (Fig. 3*D*) in contrast to WT mice (data not shown).

Systemic inflammatory profile in obese *LGALS3*$^{-/-}$ mice. Serum cytokine levels were measured to evaluate

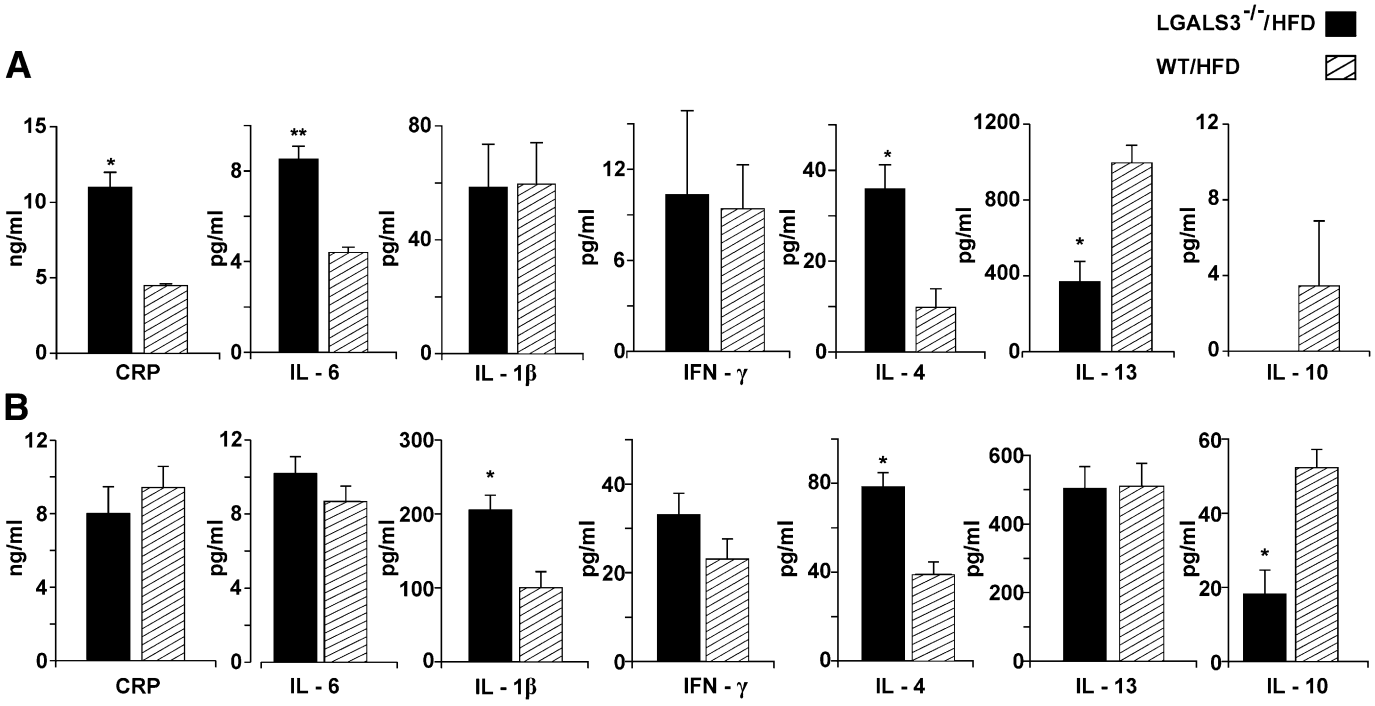

FIG. 4. Serum cytokine levels in HFD-fed *LGALS3*$^{-/-}$ and WT mice. *A*: CRP and cytokine levels in *LGALS3*$^{-/-}$ and WT mice fed HFD for 11 weeks. *B*: CRP and cytokine levels in *LGALS3*$^{-/-}$ and WT mice fed HFD for 18 weeks. The results are shown as the means ± SEM for four to six animals (11 weeks) or four to seven mice (18 weeks) per group. *P < 0.05.

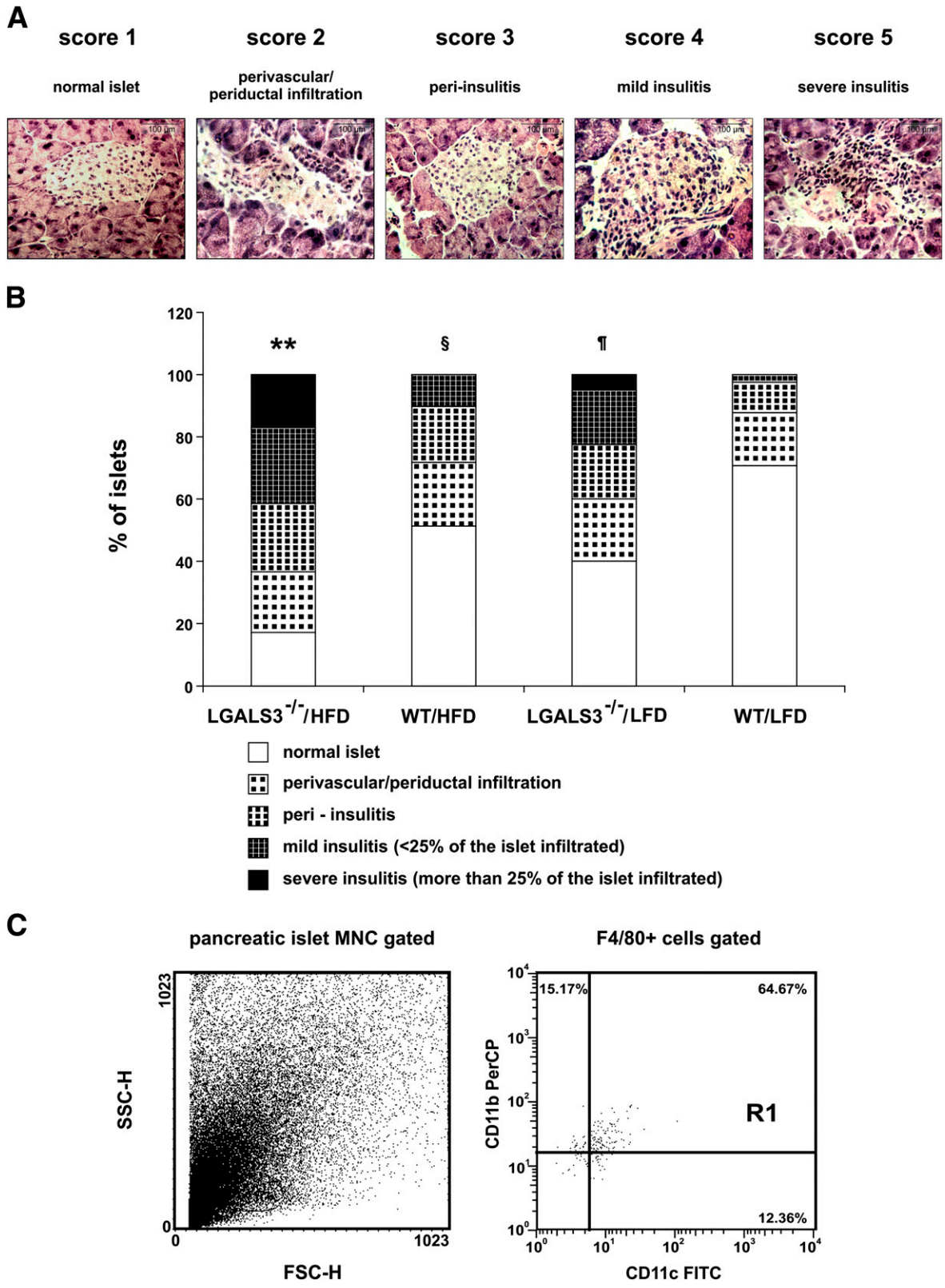

FIG. 5. Histological analysis of infiltrating mononuclear cells in pancreatic islets. *A*: Hematoxylin-eosin staining was performed on pancreatic tissue sections. Representative images of insulitis scores in *LGALS3*$^{-/-}$ mice fed HFD for 11 weeks. Original magnification ×40. Scale bars, 100 μm. *B*: Pancreatic islet inflammation (insulitis) was graded from 1 to 5, according to the extent of peri- and intraislet infiltration by mononuclear leukocytes as follows: 1, no islet infiltration; 2, peri-vascular/periductal islet infiltration; 3, peri-insulitis; 4, mild insulitis (<25% islet area infiltrated); 5, severe insulitis (>25% islet area infiltrated). *LGALS3*$^{-/-}$ mice on HFD had a significantly increased percentage of islets with severe insulitis compared with other experimental groups. *LGALS3*$^{-/-}$ mice on LFD had a significantly higher percentage of severe insulitis compared with WT mice on both diet conditions. The results are shown as percentages of islets with insulitis derived from four to six mice per group. **$P < 0.001$; ¶$P < 0.05$; §$P < 0.05$. *C*: FACS plots of mononuclear cells isolated from the pooled pancreata ($n = 5$) of *LGALS3*$^{-/-}$ mice fed HFD. The dot plots depict forward-scattered light (FSC) and side-scattered light in flow cytometry (SSC) (*left*) and the CD11b^{+}CD11c^{+} cells among gated F4/80^{+} cells (*right*). In FACS analyses, mononuclear infiltrates were not found in mice from other experimental groups. (A high-quality color representation of this figure is available in the online issue.)

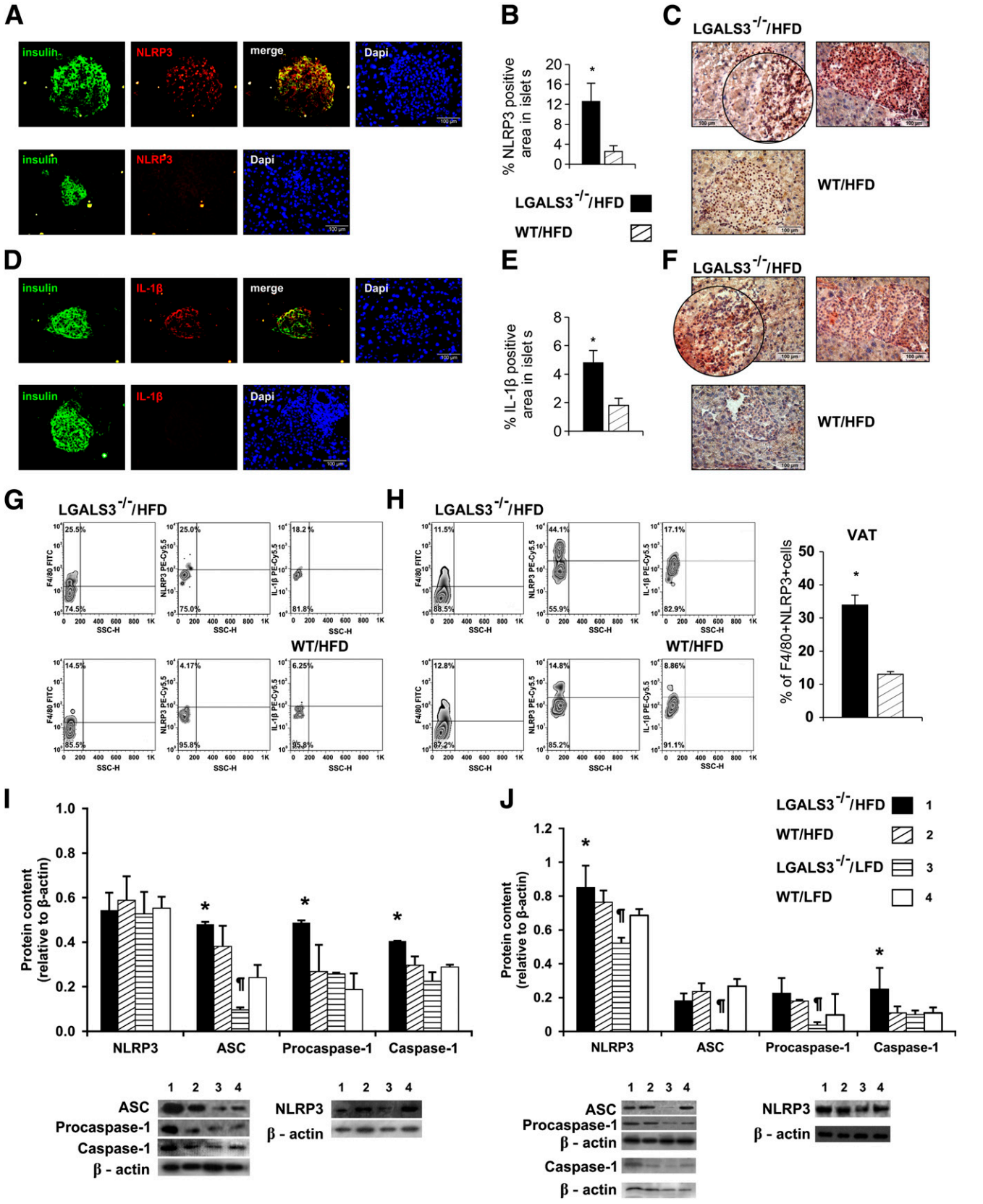

FIG. 6. Increased expression of NLRP3 inflammasome and IL-1β in pancreatic islets of *LGALS3*$^{-/-}$ mice fed HFD. *A*: Immunofluorescence staining for insulin (green) and NLRP3 inflammasome (red) together with DNA staining with DAPI (blue) in pancreatic islets from representative HFD-fed *LGALS3*$^{-/-}$ (*top*) or WT mice (*bottom*). *B*: Imunohistochemical analyses of the amount of NLRP3 inflammasome–positive areas in islets were performed on pancreatic tissue sections (four to six mice per group). *$P < 0.05$. *C*: Representative IHC staining of F4/80^{+} macrophages (brown) and NLRP3 inflammasome (red) in islets from HFD-fed *LGALS3*$^{-/-}$ or WT mice. *D*: Immunofluorescence staining for insulin (green) and IL-1β (red) together with DNA staining with DAPI (blue) in pancreatic islets from representative HFD-fed *LGALS3*$^{-/-}$ (*top*) or WT mice (*bottom*). *E*: Imunohistochemical analyses of the amount of IL-1β–positive areas in islets were performed on pancreatic tissue sections (four to six mice per

the systemic inflammatory profile in studied mice. CRP, IL-6, and IL-4 levels significantly increased in the sera of *LGALS3*$^{-/-}$ mice with HFD, whereas IL-13 and IL-10 levels significantly decreased compared with diet-matched WT mice at 11 weeks (Fig. 4*A*). After 18 weeks on HFD, IL-4 and IL-1β levels were significantly higher, whereas IL-10 levels remained significantly lower in *LGALS3*$^{-/-}$ mice (Fig. 4*B*), with no significant difference in the serum levels of IFN-γ (Fig. 4*A* and *B*) and IL-17 (data not shown) compared with WT mice.

Pronounced mononuclear cell infiltration in pancreatic islets in obese *LGALS3*$^{-/-}$ mice. Given the fact that *LGALS3*$^{-/-}$ mice exhibited obesity-related abnormalities of glucose metabolism, we performed histological analysis of the distribution of inflammatory cell infiltrate in pancreatic islets from *LGALS3*$^{-/-}$ and WT mice fed HFD or LFD for 11 weeks (Fig. 5*A*). We found significantly increased average insulitis as expressed by the insulitis score in HFD-fed *LGALS3*$^{-/-}$ mice compared with other experimental groups (Fig. 5*B*). The percentage of total intact islets and those with perivascular/periductal and peri-insulitis was 58% in *LGALS3*$^{-/-}$ mice compared with 89% in WT mice, both on HFD ($P < 0.001$). The percentages of islets with mild or severe insulitis were 24 and 17%, respectively, in HFD-fed *LGALS3*$^{-/-}$ mice compared with 10% of islets with mild insulitis and none with severe insulitis in WT mice fed HFD (both $P < 0.001$). Of note, the percentages of islets with mild or severe insulitis were 17 and 5% in LFD-fed *LGALS3*$^{-/-}$ mice compared with 2% of islets with mild insulitis ($P < 0.05$) and none with severe insulitis in WT mice fed LFD ($P < 0.05$). The percentage of islets with mild insulitis was significantly higher in HFD-fed WT mice compared with LFD-fed WT mice ($P < 0.05$).

Flow cytometric analysis of mononuclear cells isolated from digested pancreata of obese *LGALS3*$^{-/-}$ mice revealed that the majority of cells were F4/80$^+$CD11b$^+$ myeloid cells, among which the proinflammatory F4/80$^+$CD11c$^+$CD11b$^+$ BMDCs were the predominant cell type (Fig. 5*C*).

Higher incidence of NLRP3 inflammasome and IL-1β–expressing macrophages in islets and adipose tissue in obese *LGALS3*$^{-/-}$ mice. We next sought to assess NLRP3 inflammasome and IL-1β expression in pancreatic islets of mice fed HFD for 11 weeks. Immunofluorescence and morphometric immunohistochemical data showed increased NLRP3 inflammasome expression in islets of HFD-fed *LGALS3*$^{-/-}$ mice (Fig. 6*A*, *top*) compared with HFD-fed WT mice (Fig. 6*A*, *bottom*) with a significantly higher percentage of NLRP3 inflammasome–positive area in islets of obese *LGALS3*$^{-/-}$ mice (Fig. 6*B*) and prominent infiltration of F4/80$^+$ macrophages (Fig. 6*C*). Also, increased IL-1β expression in islets from obese *LGALS3*$^{-/-}$ mice (Fig. 6*D*, *top*) compared with HFD-fed WT mice (Fig. 6*D*, *bottom*) was found with a significantly higher percentage of IL-1β–positive area in islets of obese *LGALS3*$^{-/-}$ mice (Fig. 6*E* and *F*). IL-18 was not detected (data not shown). Furthermore, we show significantly higher percentages of NLRP3 inflammasome– and IL-1β–expressing macrophages derived from digested pancreatic tissue (Fig. 6*G*) and VAT (Fig. 6*H*) from HFD-fed *LGALS3*$^{-/-}$ mice compared with diet-matched WT controls.

Western blot analyses showed a similar expression of NLRP3 inflammasome in pancreata among experimental groups and significantly increased expression of ASC in HFD-fed *LGALS3*$^{-/-}$ mice compared with LFD-fed *LGALS3*$^{-/-}$ and WT mice (both $P < 0.05$). Procaspase-1 was significantly increased in HFD-fed *LGALS3*$^{-/-}$ mice compared with other experimental groups (all $P < 0.05$) and mature caspase-1 in comparison with LFD-fed *LGALS3*$^{-/-}$ mice ($P < 0.05$). ASC expression was significantly higher in HFD-fed WT mice compared with LFD-fed *LGALS3*$^{-/-}$ mice ($P < 0.05$) (Fig. 6*I*).

In VAT, a significant increase of NLRP3 inflammasome expression was found in HFD-fed *LGALS3*$^{-/-}$ mice compared with LFD-fed *LGALS3*$^{-/-}$ and WT mice (both $P < 0.05$) and increased ASC and procaspase-1 in comparison with LFD-fed *LGALS3*$^{-/-}$ mice (both $P < 0.05$). Mature caspase-1 protein expression was significantly higher in obese *LGALS3*$^{-/-}$ mice compared with other experimental groups (all $P < 0.05$). NLRP3 and ASC expression were significantly lower in LFD-fed *LGALS3*$^{-/-}$ mice compared with HFD or LFD-fed WT mice (all $P < 0.05$). Procaspase-1 was significantly lower in LFD-fed *LGALS3*$^{-/-}$ mice compared with HFD-fed WT mice ($P < 0.05$) (Fig. 6*J*).

Obese *LGALS3*$^{-/-}$ mice have higher AGE accumulation and RAGE expression in pancreatic islets. As Gal-3 has a role in the uptake and removal of metabolic compounds with proinflammatory properties related to diabetes complications, we examined the expression of AGE and RAGE in pancreatic islets. Immunofluorescence and immunohistochemical (IHC) data showed increased accumulation of AGE (Fig. 7*A* and *B*) and an increased percentage of RAGE-positive area in islets in *LGALS3*$^{-/-}$ mice fed HFD for 11 weeks compared with diet-matched WT mice (Fig. 7*C* and *D*).

We show increased expression of Gal-3 protein in the pancreatic islets of HFD-fed WT mice compared with LFD-fed WT mice at 11 weeks (Fig. 7*E*).

NLRP3 inflammasome expression and caspase-1–dependent IL-1β production are increased in stimulated peritoneal macrophages in *LGALS3*$^{-/-}$ compared with WT mice. We demonstrate the inherent genotype differences in the cellular response of *LGALS3*$^{-/-}$ mice vs. WT mice as LPS (100 ng/mL), palmitate-BSA (100 μmol/L), and LPS plus palmitate induced significantly higher IL-1β and IL-6 production in *LGALS3*$^{-/-}$ peritoneal macrophages (Fig. 8*A*). IL-1β production was significantly reduced in the presence of the caspase-1 inhibitor Z-YVAD-FMK (10 μmol/L), whereas

group). *$P < 0.05$. *F*: Representative IHC staining of F4/80$^+$ macrophages (brown) and IL-1β (red) in islets from HFD-fed *LGALS3*$^{-/-}$ or WT mice. *G*: Representative FACS plot of F4/80$^+$NLRP3$^+$ and F4/80$^+$IL-1β$^+$ macrophages in the pancreas of HFD-fed *LGALS3*$^{-/-}$ and WT mice. *H*: Representative FACS plot of F4/80$^+$NLRP3$^+$ and F4/80$^+$IL-1β$^+$ macrophages in VAT of HFD-fed *LGALS3*$^{-/-}$ and WT mice. Significantly increased percentage of F4/80$^+$NLRP3$^+$ macrophages in HFD-fed *LGALS3*$^{-/-}$ vs. WT mice. *$P < 0.05$. *I*: Western blot analyses of NLRP3, ASC, procaspase-1, and caspase-1 expression in the pancreas. HFD-fed *LGALS3*$^{-/-}$ mice had significantly higher ASC expression when compared with LFD-fed *LGALS3*$^{-/-}$ and WT mice, significantly higher procaspase-1 expression when compared with all experimental groups, and significantly higher active caspase-1 expression when compared with *LGALS3*$^{-/-}$ mice fed LFD (all *$P < 0.05$). ASC expression was significantly higher in HFD-fed WT mice compared with LFD-fed LGALS3$^{-/-}$ mice. ¶$P < 0.05$. *J*: Western blot analyses of NLRP3, ASC, procaspase-1, and caspase-1 expression in VAT. *LGALS3*$^{-/-}$ mice on HFD showed significantly increased expression of NLRP3 when compared with LFD-fed *LGALS3*$^{-/-}$ and WT mice and significantly increased expression of active caspase-1 when compared with all experimental groups (all *$P < 0.05$). NLRP3 and ASC expression were significantly lower in LFD-fed *LGALS3*$^{-/-}$ mice compared with HFD or LFD-fed WT mice (all ¶$P < 0.05$). Procaspase-1 was significantly lower in LFD-fed *LGALS3*$^{-/-}$ mice compared with HFD-fed WT mice. ¶$P < 0.05$. The results are representative of two to three repeated experiments.

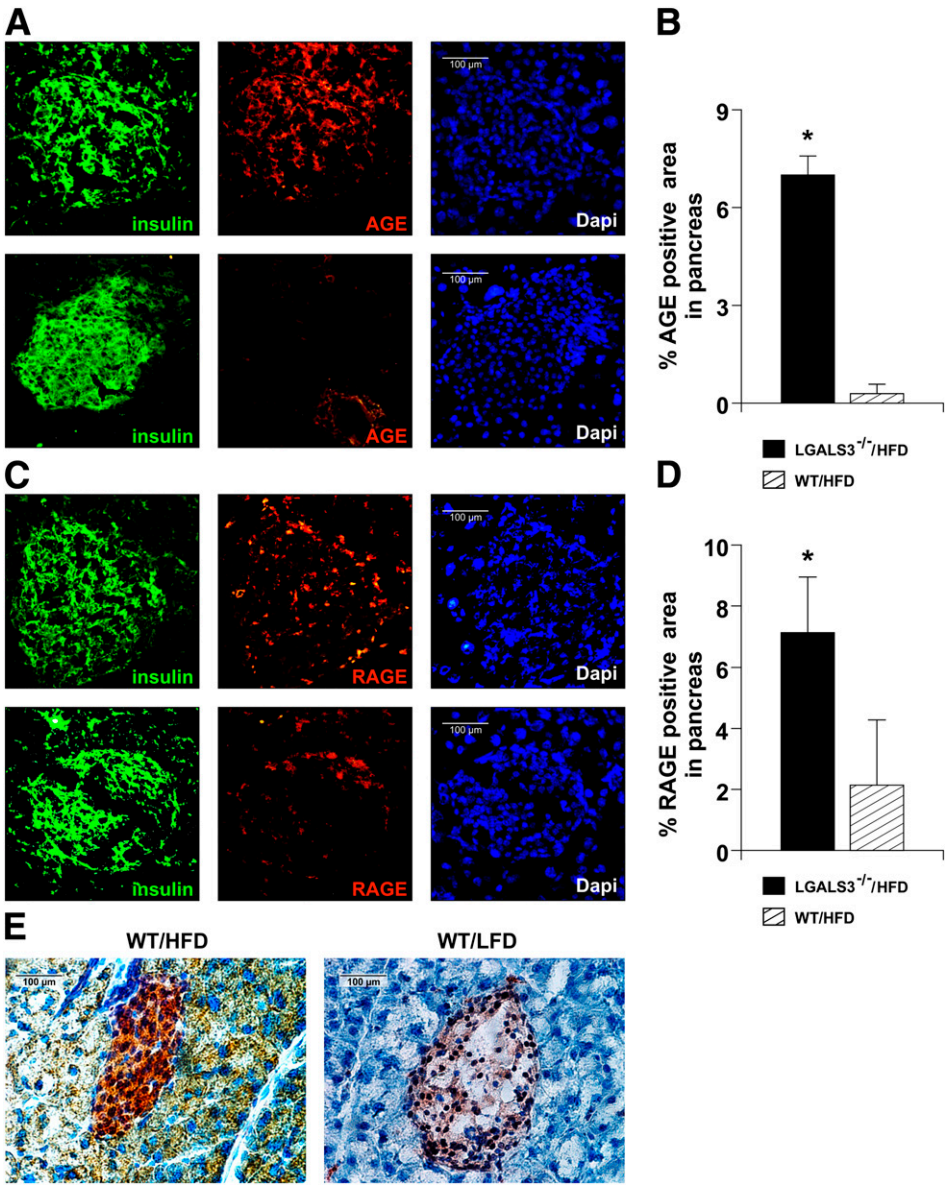

FIG. 7. Increased expression of AGE and RAGE in pancreatic islets of HFD-fed *LGALS3*$^{-/-}$ mice. *A*: Immunofluorescence staining for insulin (green) and AGE (red) together with DNA staining with DAPI (blue) in pancreatic islets from representative *LGALS3*$^{-/-}$ (*top*) and WT mice fed an HFD (*bottom*). *B*: Evaluation of % AGE-positive areas was performed on IHC-stained tissue sections from four to six mice per group. *C*: Immunofluorescence staining for insulin (green) and RAGE (red) together with DNA staining with DAPI (blue) in pancreatic islets from representative *LGALS3*$^{-/-}$ (*top*) and WT mice fed an HFD (*bottom*). *D*: Evaluation of % RAGE-positive areas was performed on IHC-stained tissue sections from four to six mice per group. *E*: Representative IHC image of Gal-3 expression in HFD- or LFD-fed WT mice. The results are representative of two to three repeated experiments. *$P < 0.05$.

IL-6 production was not affected (Fig. 8*A*). No significant difference in IL-1β production between *LGALS3*$^{-/-}$ and WT mice was observed when cells were stimulated with high glucose or H_2O_2 with and without priming with LPS (data not shown).

In vitro stimulation of cells with LPS or palmitate significantly increased percentages of NLRP3 inflammasome–expressing F4/80$^+$ macrophages (Fig. 8*B*) and significantly increased caspase-1 activity (Fig. 8*C*) in *LGALS3*$^{-/-}$ compared with WT macrophages. Transfection of *LGALS3*$^{-/-}$ peritoneal macrophages with NLRP3 siRNA resulted in a significant reduction of the NLRP3 inflammasome expression compared with cells transfected with control siRNA (15.6 vs. 3.7%) (Fig. 8*D*). Transfection with NLRP3 siRNA, but not with control siRNA, led to a significant decrease in IL-1β production by *LGALS3*$^{-/-}$ macrophages stimulated with palmitate alone and LPS plus palmitate (Fig. 8*D*).

Increased activation of NF-κB in *LGALS3*$^{-/-}$ mice. We next tested for the differences in NF-κB activation in *LGALS3*$^{-/-}$ vs. WT mice by using an antibody against the NF-κB p65 subunit phosphorylated at the amino acid residue serine 536, an activated form of NF-κB that is induced in response to a variety of proinflammatory stimuli, including LPS. Figure 8*E* represents the percentage of phospho–NF-κB p65–expressing peritoneal macrophages in response to LPS (1 μg/mL) with and without palmitate (100 μmol/L). A significant increase of phospho–NF-κB p65–expressing F4/80$^+$ macrophages in *LGALS3*$^{-/-}$ compared with WT cells in response to LPS and LPS plus palmitate was observed (Fig. 8*E*).

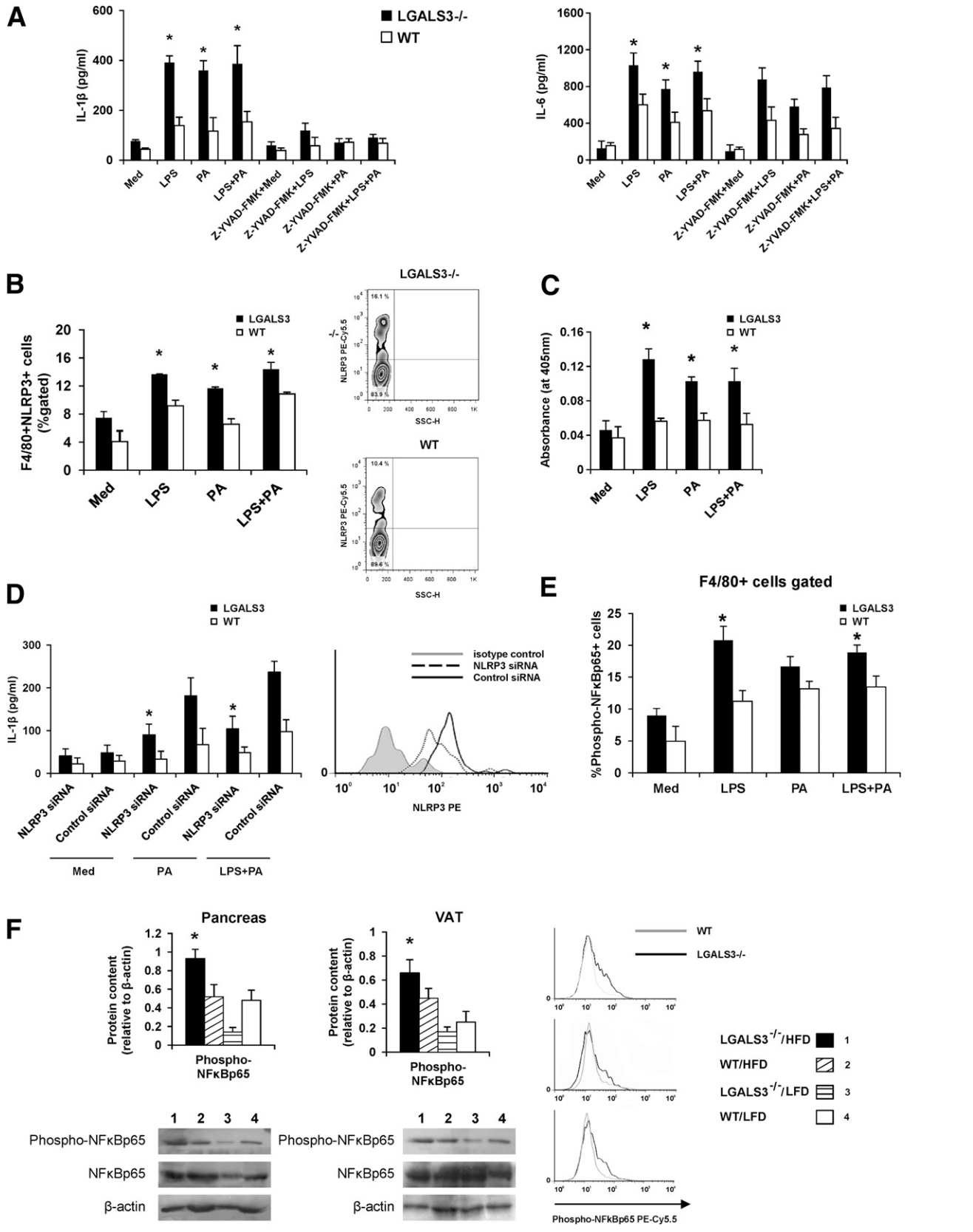

FIG. 8. Stimulated *LGALS3*$^{-/-}$ peritoneal macrophages have increased NLRP3 inflammasome expression, caspase-1–dependent IL-1β production, and higher expression of phosphorylated NF-κB p65. *A*: Significantly higher production of IL-1β by *LGALS3*$^{-/-}$ vs. WT peritoneal macrophages upon simulation with LPS (100 ng), palmitate-BSA (PA-BSA) (100 μmol/L), or LPS plus PA, whereas the production was significantly reduced in the presence of the caspase-1 inhibitor Z-YVAD (10 μmol/L). *LGALS3*$^{-/-}$ macrophages stimulated with LPS, PA, or LPS plus PA produce more IL-6 when compared with WT macrophages, and the production was not affected by caspase-1 inhibitor Z-YVAD. *B*: Significantly increased percentage of F4/80^{+}NLRP3^{+} macrophages in *LGALS3*$^{-/-}$ vs. WT mice when stimulated with LPS, PA-BSA, or LPS plus PA. Representative FACS plot of F4/80^{+}NLRP3^{+} peritoneal macrophages in *LGALS3*$^{-/-}$ and WT mice. *C*: Significantly increased caspase-1 activity in cell lysates of *LGALS3*$^{-/-}$

Western blotting showed significantly increased expression of phospho–NF-κB p65 in pancreata of *LGALS3*$^{-/-}$ fed HFD for 18 weeks compared with other experimental groups (all $P < 0.05$) (Fig. 8*F*). Phospho/total ratio of NF-κB p65 was the highest in the pancreata of HFD-fed *LGALS3*$^{-/-}$ mice (0.816) compared with HFD-fed WT mice (0.413) and LFD-fed *LGALS3*$^{-/-}$ mice (0.120) or WT animals (0.345). In VAT, phospho–NF-κB p65 expression was significantly higher in HFD-fed *LGALS3*$^{-/-}$ mice compared with LFD-fed *LGALS3*$^{-/-}$ mice ($P < 0.05$) (Fig. 8*F*). Phospho/total ratio of NF-κB p65 was the highest in the VAT of HFD-fed *LGALS3*$^{-/-}$ mice (0.842) compared with HFD-fed WT mice (0.469) and LFD-fed *LGALS3*$^{-/-}$ mice (0.370) or WT animals (0.272).

DISCUSSION

This study provides evidence that knockdown of Gal-3 results in accelerated HFD-induced obesity and diabetes, as indicated by the significantly higher body weight and total VAT weight, hyperglycemia, increased HOMA-IR, severe insulitis, and pronounced infiltration of pancreatic islets with proinflammatory macrophages. Ongoing inflammation in largely expanded adipose tissue in obese *LGALS3*$^{-/-}$ mice was characterized by the increased incidence of type 1 CD3$^+$ T and CD3$^+$NK1.1$^+$ NKT lymphocytes expressing IFN-γ. Th1 effector cells have a major role in obesity-associated chronic inflammation (26), and NKT cell depletion prevents diet-induced metaflammation and glucose intolerance (27). Reduced adipose tissue and splenic Tregs in obese *LGALS3*$^{-/-}$ mice are in line with the data of depleted adipose tissue Tregs during obesity (28). HFD increased the incidence of activated CD4$^+$PD-1$^+$ T cells in VAT and spleens in *LGALS3*$^{-/-}$ mice, possibly due to enhanced TCR-mediated signaling in T cells in Gal-3 deficiency (10,29).

F4/80$^+$CD11c$^+$CD206$^+$ macrophages, increased in the VAT of obese *LGALS3*$^{-/-}$ mice, were recently described as a novel macrophage subset to facilitate adipose tissue inflammation and insulin resistance in obese human subjects (30). Eighteen weeks of HFD in the VAT of *LGALS3*$^{-/-}$ mice increased proinflammatory F4/80$^+$CD11b$^+$CD11c$^+$ BMDCs, cells that have a crucial role in obesity-induced inflammation (31). Markedly reduced alternatively activated M2 macrophages in the VAT of *LGALS3*$^{-/-}$ mice are in line with the reported data of Gal-3 involvement in the polarization of M2 macrophages (32,33).

Accelerated HFD-induced obesity in Gal-3–deficient mice was associated with systemic inflammation. Increased IL-6 and IL-1β induced by HFD in *LGALS3*$^{-/-}$ mice are in line with the data of increased production of IL-1β and IL-6 in Gal-3–deficient macrophages during infection (34). Increased systemic IL-4 might indicate enhanced T-cell function during nutrient excess in *LGALS3*$^{-/-}$ mice as Gal-3–deficient CD4$^+$ T cells were shown to produce increased amounts of IFN-γ and IL-4 after T-cell receptor engagement (35). Lack of Gal-3 on dendritic cells favors lower IL-10 production and increased IFN-γ by allogeneic T cells (36). Reduced levels of IL-13 and IL-10 in the sera of obese *LGALS3*$^{-/-}$ mice might contribute to amplified obesity-induced inflammation. IL-10 has a protective role in type 2 diabetes by increasing insulin sensitivity in skeletal muscle (37).

The most striking finding in our study was the presence of severe insulitis in obese *LGALS3*$^{-/-}$ mice, but also in lean *LGALS3*$^{-/-}$ mice. Enhanced expression of Gal-3 protects rat pancreatic β-cells from the cytotoxic effect of IL-1β (18), and Gal-3 is highly expressed in islet endothelial cells in obesity-induced diabetes in mice (19), but its role in diabetes progression still remains to be elucidated. Moreover, we show upregulation of Gal-3 protein in pancreatic islets in HFD-fed WT mice. F4/80$^+$CD11c$^+$CD11b$^+$ BMDCs were the most abundant cell type in islet infiltrates in obese *LGALS3*$^{-/-}$ mice, and higher expression of NLRP3 inflammasome and IL-1β in F4/80$^+$ macrophages reflects ongoing inflammation in islets of HFD-fed *LGALS3*$^{-/-}$ mice. Apart from macrophages, β-cells could produce IL-1β when exposed to proinflammatory metabolic signals, possibly through NLRP3 inflammasome activation (38). Most recently, type 2 diabetes has been considered an autoinflammatory disease with the central role for NLRP3-ASC inflammasome–mediated IL-1β production (39,40). We did not find a significant increase in protein content of NLRP3 inflammasome in whole-tissue lysates of pancreas and VAT in HFD-fed *LGALS3*$^{-/-}$ mice compared with HFD-fed WT mice. However, a trend toward increased ASC and NLRP3 inflammasome protein content was found in pancreas and VAT, respectively. The increased mature caspase-1 protein expression found in the VAT of obese *LGALS3*$^{-/-}$ mice might indicate increased NLRP3 inflammasome activation in adipose tissue in Gal-3 deficiency. In fact, *LGALS3*$^{-/-}$ macrophages produced increased amounts of IL-1β, which was caspase-1 dependent, and had increased NLRP3 inflammasome expression and higher caspase-1 activity in response to LPS and/or palmitate compared with WT cells. In addition, silencing of NLRP3 by siRNA attenuated IL-1β production by *LGALS3*$^{-/-}$ macrophages, suggestive of the enhanced NLRP3 inflammasome activation in Gal-3–deficient mice. The most recent study shows that NLRP3 expression is increased by TLR agonists, including LPS, in murine macrophages in an NF-κB–dependent manner (41). Moreover, *LGALS3*$^{-/-}$ macrophages produced increased amounts of IL-1β and IL-6 in response to LPS stimulation, which is line with the evidence of markedly elevated LPS-induced proinflammatory cytokines in Gal-3–deficient macrophages since Gal-3 binds LPS and prevents its activity (42). HFD strongly increases intestinal permeability and increases blood levels of endotoxin (43). Endotoxin, free fatty acids, and AGE, through TLRs and RAGE, activate NF-κB and lead to IL-1β and tumor necrosis factor-α production, thus promoting insulin resistance (39,44). *LGALS3*$^{-/-}$ macrophages had increased expression of

peritoneal macrophages stimulated with LPS (100 ng), PA (100 μmol/L), or LPS plus PA in comparison with WT peritoneal macrophages. *D*: Significantly reduced palmitate (100 μmol/L) and LPS (100 ng) plus palmitate (100 μmol/L) stimulated IL-1β production from *LGALS3*$^{-/-}$ macrophages transfected with NLRP3 siRNA compared with cells treated with control siRNA. Representative histogram of NLRP3 expression in macrophages transfected with NLRP3 siRNA or control siRNA. *E*: Significantly increased expression of phosphorylated NF-κB p65 in *LGALS3*$^{-/-}$ macrophages stimulated with LPS (1 μg/mL) and LPS plus PA (100 μmol/L) when compared with WT macrophages. Representative histograms of F4/80$^+$ macrophages expressing NF-κB p65 (phospho-S536) in *LGALS3*$^{-/-}$ and WT mice. *F*: Western blot analyses of NF-κB p65 and phospho–NF-κB p65 expression in the pancreas and VAT. HFD-fed *LGALS3*$^{-/-}$ mice have significantly increased expression of phosphorylated NF-κB p65 when compared with all experimental groups in the pancreas and compared with LFD-fed *LGALS*$^{-/-}$ and WT mice in VAT. All experimental groups have a similar expression of total NF-κB p65 in the pancreas and VAT. The results are representative of two to three repeated experiments. *$P < 0.05$.

phospho–NF-κB p65 in response to LPS, which complements the reported data (45). Increased pancreatic and also VAT phospho–NF-κB p65 expression could be related to increased accumulation of AGE and upregulation of RAGE in islets of *LGALS3*$^{-/-}$ mice fed HFD. These findings indicate that additional NF-kB–mediated proinflammatory pathways (46) might operate in amplified obesity-induced inflammation in *LGALS3*$^{-/-}$ mice.

Collectively, the amplified obesity-induced inflammation in adipose tissue and pancreatic islets in *LGALS3*$^{-/-}$ mice suggest a protective role for Gal-3 in obesity and type 2 diabetes, which could be of therapeutic relevance.

ACKNOWLEDGMENTS

This work was supported by grants from the Serbian Ministry of Science and Technological Development (175071 and 175069) (Belgrade, Serbia).

No potential conflicts of interest relevant to this article were reported.

N.N.P. and J.M.P. researched data and wrote the manuscript. I.P.J., G.D.R., M.Z.M., and I.G.N. researched data. N.S.Z. and A.L.D. researched data and contributed to discussion. N.N.A. reviewed and edited the manuscript. M.L.L. contributed to discussion and reviewed and edited the manuscript. M.L.L. is the guarantor of this work and, as such, had full access to all the data in the study and takes responsibility for the integrity of the data and the accuracy of the data analysis.

We would like to thank Milan Milojevic, Dragana Djurdjevic, and Ivana Milovanovic (Center for Molecular Medicine and Stem Cell Research) and Dragana Djacic (University of Kragujevac) for technical assistance.

REFERENCES

1. Lumeng CN, Saltiel AR. Inflammatory links between obesity and metabolic disease. J Clin Invest 2011;121:2111–2117
2. Feuerer M, Herrero L, Cipolletta D, et al. Lean, but not obese, fat is enriched for a unique population of regulatory T cells that affect metabolic parameters. Nat Med 2009;15:930–939
3. Nishimura S, Manabe I, Nagasaki M, et al. CD8+ effector T cells contribute to macrophage recruitment and adipose tissue inflammation in obesity. Nat Med 2009;15:914–920
4. Weisberg SP, McCann D, Desai M, Rosenbaum M, Leibel RL, Ferrante AW Jr. Obesity is associated with macrophage accumulation in adipose tissue. J Clin Invest 2003;112:1796–1808
5. Xu H, Barnes GT, Yang Q, et al. Chronic inflammation in fat plays a crucial role in the development of obesity-related insulin resistance. J Clin Invest 2003;112:1821–1830
6. Sriwijitkamol A, Christ-Roberts C, Berria R, et al. Reduced skeletal muscle inhibitor of kappaB β content is associated with insulin resistance in subjects with type 2 diabetes: reversal by exercise training. Diabetes 2006; 55:760–767
7. Wen H, Gris D, Lei Y, et al. Fatty acid-induced NLRP3-ASC inflammasome activation interferes with insulin signaling. Nat Immunol 2011;12:408–415
8. Vandanmagsar B, Youm YH, Ravussin A, et al. The NLRP3 inflammasome instigates obesity-induced inflammation and insulin resistance. Nat Med 2011;17:179–188
9. Stienstra R, van Diepen JA, Tack CJ, et al. Inflammasome is a central player in the induction of obesity and insulin resistance. Proc Natl Acad Sci USA 2011;108:15324–15329
10. Hsu DK, Chen HY, Liu FT. Galectin-3 regulates T-cell functions. Immunol Rev 2009;230:114–127
11. Jiang H-R, Al Rasebi Z, Mensah-Brown E, et al. Galectin-3 deficiency reduces the severity of experimental autoimmune encephalomyelitis. J Immunol 2009;182:1167–1173
12. Mensah-Brown EP, Al Rabesi Z, Shahin A, et al. Targeted disruption of the galectin-3 gene results in decreased susceptibility to multiple low dose streptozotocin-induced diabetes in mice. Clin Immunol 2009;130:83–88
13. Volarevic V, Milovanovic M, Ljujic B, et al. Galectin-3 deficiency prevents concanavalin A-induced hepatitis in mice. Hepatology 2012;55:1954–1964
14. Radosavljevic G, Jovanovic I, Majstorovic I, et al. Deletion of galectin-3 in the host attenuates metastasis of murine melanoma by modulating tumor adhesion and NK cell activity. Clin Exp Metastasis 2011;28:451–462
15. Zhu W, Sano H, Nagai R, Fukuhara K, Miyazaki A, Horiuchi S. The role of galectin-3 in endocytosis of advanced glycation end products and modified low density lipoproteins. Biochem Biophys Res Commun 2001;280:1183–1188
16. Pugliese G, Pricci F, Iacobini C, et al. Accelerated diabetic glomerulopathy in galectin-3/AGE receptor 3 knockout mice. FASEB J 2001;15:2471–2479
17. Iacobini C, Menini S, Ricci C, et al. Accelerated lipid-induced atherogenesis in galectin-3-deficient mice: role of lipoxidation via receptor-mediated mechanisms. Arterioscler Thromb Vasc Biol 2009;29:831–836
18. Karlsen AE, Størling ZM, Sparre T, et al. Immune-mediated beta-cell destruction in vitro and in vivo-A pivotal role for galectin-3. Biochem Biophys Res Commun 2006;344:406–415
19. Darrow AL, Shohet RV, Maresh JG. Transcriptional analysis of the endothelial response to diabetes reveals a role for galectin-3. Physiol Genomics 2011;43:1144–1152
20. Matthews DR, Hosker JP, Rudenski AS, Naylor BA, Treacher DF, Turner RC. Homeostasis model assessment: insulin resistance and beta-cell function from fasting plasma glucose and insulin concentrations in man. Diabetologia 1985;28:412–419
21. Boitard C, Debray-Sachs M, Pouplard A, Assan R, Hamburger J. Lymphocytes from diabetics suppress insulin release in vitro. Diabetologia 1981;21: 41–46
22. Chan WL, Pejnovic N, Hamilton H, et al. Atherosclerotic abdominal aortic aneurysm and the interaction between autologous human plaque-derived vascular smooth muscle cells, type 1 NKT, and helper T cells. Circ Res 2005;96:675–683
23. Hall TR, Bogdani M, Leboeuf RC, et al. Modulation of diabetes in NOD mice by GAD65-specific monoclonal antibodies is epitope specific and accompanied by anti-idiotypic antibodies. Immunology 2008;123:547–554
24. Lohmann C, Schäfer N, von Lukowicz T, et al. Atherosclerotic mice exhibit systemic inflammation in periadventitial and visceral adipose tissue, liver, and pancreatic islets. Atherosclerosis 2009;207:360–367
25. Saksida T, Stosic-Grujicic S, Timotijevic G, Sandler S, Stojanovic I. Macrophage migration inhibitory factor deficiency protects pancreatic islets from palmitic acid-induced apoptosis. Immunol Cell Biol 2012;90:688–698
26. Strissel KJ, DeFuria J, Shaul ME, Bennett G, Greenberg AS, Obin MS. T-cell recruitment and Th1 polarization in adipose tissue during diet-induced obesity in C57BL/6 mice. Obesity (Silver Spring) 2010;18:1918–1925
27. Ohmura K, Ishimori N, Ohmura Y, et al. Natural killer T cells are involved in adipose tissues inflammation and glucose intolerance in diet-induced obese mice. Arterioscler Thromb Vasc Biol 2010;30:193–199
28. Ilan Y, Maron R, Tukpah AM, et al. Induction of regulatory T cells decreases adipose inflammation and alleviates insulin resistance in ob/ob mice. Proc Natl Acad Sci USA 2010;107:9765–9770
29. Francisco LM, Sage PT, Sharpe AH. The PD-1 pathway in tolerance and autoimmunity. Immunol Rev 2010;236:219–242
30. Wentworth JM, Naselli G, Brown WA, et al. Pro-inflammatory CD11c +CD206+ adipose tissue macrophages are associated with insulin resistance in human obesity. Diabetes 2010;59:1648–1656
31. Nguyen MTA, Favelyukis S, Nguyen A-K, et al. A subpopulation of macrophages infiltrates hypertrophic adipose tissue and is activated by free fatty acids via Toll-like receptors 2 and 4 and JNK-dependent pathways. J Biol Chem 2007;282:35279–35292
32. Lumeng CN, Bodzin JL, Saltiel AR. Obesity induces a phenotypic switch in adipose tissue macrophage polarization. J Clin Invest 2007;117:175–184
33. MacKinnon AC, Farnworth SL, Hodkinson PS, et al. Regulation of alternative macrophage activation by galectin-3. J Immunol 2008;180:2650–2658
34. Ferraz LC, Bernardes ES, Oliveira AF, et al. Lack of galectin-3 alters the balance of innate immune cytokines and confers resistance to *Rhodococcus equi* infection. Eur J Immunol 2008;38:2762–2775
35. Chen HY, Fermin A, Vardhana S, et al. Galectin-3 negatively regulates TCR-mediated CD4+ T-cell activation at the immunological synapse. Proc Natl Acad Sci USA 2009;106:14496–14501
36. Mobergslien A, Sioud M. Galectin-1 and -3 gene silencing in immature and mature dendritic cells enhances T cell activation and interferon-γ production. J Leukoc Biol 2012;91:461–467
37. Hong EG, Ko HJ, Cho YR, et al. Interleukin-10 prevents diet-induced insulin resistance by attenuating macrophage and cytokine response in skeletal muscle. Diabetes 2009;58:2525–2535
38. Donath MY, Shoelson SE. Type 2 diabetes as an inflammatory disease. Nat Rev Immunol 2011;11:98–107
39. Schroder K, Zhou R, Tschopp J. The NLRP3 inflammasome: a sensor for metabolic danger? Science 2010;327:296–300

40. Dinarello CA, Donath MY, Mandrup-Poulsen T. Role of IL-1β in type 2 diabetes. Curr Opin Endocrinol Diabetes Obes 2010;17:314–321
41. Qiao Y, Wang P, Qi J, Zhang L, Gao C. TLR-induced NF-κB activation regulates NLRP3 expression in murine macrophages. FEBS Lett 2012;586: 1022–1026
42. Li Y, Komai-Koma M, Gilchrist DS, et al. Galectin-3 is a negative regulator of lipopolysaccharide-mediated inflammation. J Immunol 2008;181:2781–2789
43. Cani PD, Bibiloni R, Knauf C, et al. Changes in gut microbiota control metabolic endotoxemia-induced inflammation in high-fat diet-induced obesity and diabetes in mice. Diabetes 2008;57:1470–1481
44. Sakurai H, Suzuki S, Kawasaki N, et al. Tumor necrosis factor-alpha-induced IKK phosphorylation of NF-kappaB p65 on serine 536 is mediated through the TRAF2, TRAF5, and TAK1 signaling pathway. J Biol Chem 2003;278:36916–36923
45. Iacobini C, Menini S, Oddi G, et al. Galectin-3/AGE-receptor 3 knockout mice show accelerated AGE-induced glomerular injury: evidence for a protective role of galectin-3 as an AGE receptor. FASEB J 2004;18:1773–1775
46. Yan SF, Ramasamy R, Schmidt AM. Mechanisms of disease: advanced glycation end-products and their receptor in inflammation and diabetes complications. Nat Clin Pract Endocrinol Metab 2008;4:285–293